Iranian Journal of Medical Physics

ijmp.mums.ac.ir

Calculation of Involved and Noninvolved Organs Doses in Carbon Therapy of Brain Tumor Using GEANT4 Simulation Toolkit

Maria Ahmadi[1], S. Mohammad Motevalli[1*], Payvand Taherparvar[2], Vahid Zanganeh[3]

1. Department of Physics, Faculty of Science, University of Mazandaran, Babolsar, Iran
2. Department of Physics, Faculty of Science, University of Guilan, Rasht, Iran
3. Department of Physics, Faculty of Science, Golestan University, Gorgan, Iran

ARTICLE INFO

Article type:
Original Paper

Article history:
Received: Mar 01, 2023
Accepted: Aug 22, 2023

Keywords:
Heavy Ion Radiotherapy
Brain
Monte Carlo Simulation
SOBP

ABSTRACT

Introduction: This study used the GEANT4 Monte Carlo toolkit for radiation transport simulations in brain carbon therapy, incorporating a human phantom model to accurately assess dose delivery to targeted and non-targeted organs. Weight factors were employed to generate a Spread Out Bragg Peak (SOBP).

Material and Methods: The study used the ORNL-MIRD phantom to simulate carbon therapy for brain tumors, finding that the optimal energy range for carbon ions was 2420-2560 MeV to effectively cover the tumor. To achieve a homogeneous radiation dose, a Spread Out ragg Peak (SOBP) was generated using multiple Bragg peaks with specific intensity factors. Beam parameters were also evaluated per ICRU guidelines.

Results: This study estimated the flux and dose distributions of secondary particles—protons, electrons, neutrons, alpha particles, and photons—in the brain tumor and surrounding tissues. We calculated the cumulative dose from both carbon ions and secondary particles, finding an absorbed dose ratio of 0.003 in healthy brain tissue compared to the tumor, with values of 4.8×10^{-4} for the skull and 2.6×10^{-5} for the thyroid. Notably, neutrons and photons can significantly increase energy transfer to distant organs, raising secondary cancer risk.

Conclusion: The findings presented in this article demonstrated that the involvement of secondary particles in the dose received by both the brain and other organs remains minimal, as the highest absorbed dose was predominantly localized within the tumor.

►*Please cite this article as:*
Ahmadi M, Motevalli SM, Taherparvar P, Zanganeh V. Calculation of Involved and Noninvolved Organs Doses in Carbon Therapy of Brain Tumor Using GEANT4 Simulation Toolkit. Iran J Med Phys 2024; 21: 287-294. 10.22038/ijmp.2023.71006.2251.

Introduction

In recent years, particle therapy has gained popularity for treating various cancers and tumors. However, despite advancements in radiation therapy technology, a significant challenge remains: the rapid decrease in photon fluence with increasing tissue penetration depth. This decrease results in substantial doses being delivered to healthy organs before and after the target region due to photon interactions. To address this issue, there is increasing interest in using therapeutic beams like protons and carbon ions. The primary aim of radiation therapy is to maximize the dose to the tumor while minimizing exposure to surrounding healthy tissues. Notably, particle radiation therapy, particularly carbon ion radiotherapy, has demonstrated greater efficacy in achieving this objective compared to other radiotherapy methods[1-3]. In recent years, researchers have investigated the dosimetric properties of hadrons like carbons for the treatment of various malignancies. Compared to photons and electrons, carbon ion beams offer several benefits, such as fewer Coulomb interactions than protons and sharper lateral penumbra, resulting in a fast dose fall at the end of the carbon beam range [4-10]. Charged particle therapy is a treatment method that uses either carbon ions or protons to deliver radiation directly to cancerous tumors. This approach selectively targets and damages cancer cells, while minimizing harm to surrounding healthy tissue and vital organs. Carbon ions are particularly effective in treating tumors that are located near or within critical organs, such as the eyes, lungs, and esophagus. Additionally, this type of therapy is suitable for children with cancer. One major advantage of carbon ion therapy is its high level of accuracy in targeting and destroying cancerous tumors, even those that are difficult to access due to their location in the head and neck region. This is especially important given the anatomic constraints of this area. By delivering a focused dose of radiation directly to the tumor, carbon

*Corresponding Author: Tel: +98-1135302480; Email: motavali@umz.ac.ir

therapy can minimize the acute toxicity profile associated with traditional head and neck cancer treatments that require irradiation. Moreover, it may also be appropriate for patients who have received multiple prior courses of radiation therapy [11, 12]. This kind of ions has higher relative biological effectiveness (RBE) compared with protons or photons that is relevant to their ability to create more complicated DNA damages. The complex DNA damages can increase tumor kill because the cell repair ability decreases [12]. Heavy particles such as carbon ions transfer their energy in matter as a function of depth. In common radiotherapy, most of the photon's energy deposits near the skin surface. Although, photons deposit their maximum dose near to the skin surface, carbon ions have a low dose when entering the tissue and then most of the energy deposit at a well-defined depth which called Bragg peak at the tumor region with a relatively well-defined range [13]. By calculating the beam weighting factors for different energies, the tumor volume can be irradiated with a Spread Out Bragg Peak (SOBP) and no exit dose [14-17]. Monte Carlo calculations using different codes such as GEANT4 toolkit allow simulation of carbon ion interactions with different materials in the cancer treatment energy interval. The accessibility of computational power with high statistical precision is increased that made it possible to carry out simulations of carbon ion therapy treatment planning. This kind of simulation has been demonstrated as a valuable tool for the development of different methods to predict dose calculations in the patient for clinical practices [18, 19].

Some Monte Carlo simulation codes that are suitable for charge particle simulation are including EGSnrc [20], BEAMnrc, MCNPX [21], and GEANT4 [19, 22]. GEANT4 is a popular toolkit that has been used by a large number of projects in a variety of applications, including high energy physics, medical physics, and radiation protection. GEANT4 is open source and has a very high ability to transport all particles relevant to radiation therapy applications, with an abundant set of physics models based on experimental data and also has a powerful capability to describe complex geometry. The advantage of GEANT4 over other simulation tools is its powerful geometry and physics modelling in an advanced computing environment. Pristine Bragg Peaks resulting from carbon ion interactions were simulated using electromagnetic and hadronic interactions by GEANT4 environment [23-24].

In recent decades, G. Kraft studied tumor therapy with ion beams [25]. Shinnosuke Matsumoto et al. estimated out of field doses during carbon ion radiotherapy for pediatric cerebellar ependymoma [26]. Yusuke Demizu et al. evaluated the efficacy and toxicity of particle therapy using proton or carbon ions for unresectable or incompletely resected pelvic bone and soft tissue sarcomas [27]. Other studies, Hirokazu Makishima et al. conducted a prospective single arm dose escalation study since 2006 for colorectal cancer liver metastasis using single fraction carbon ion radiotherapy [28]. Ganjeh in 2019 & Yonai in 2021, studied the effect of large rate of secondary neutrons in carbon ion radiotherapy and proton therapy during liver cancer, prostate cancer and pediatric brain tumor treatments through the Monte Carlo simulation and experimental. They showed that secondary neutrons in the distant area from the target volume are the major source in carbon ion radiotherapy [29].

In this study, we investigated brain carbon ion therapy utilizing a GEANT4-based Monte Carlo simulation technique. Our objective was to assess the absorbed dose of secondary particles in non-target organs adjacent to the target volume through the Monte Carlo simulation approach. This methodology involves computing the absorbed dose of secondary particles within the examined organs. The primary objective was to estimate the overall side effects resulting by the absorbed dose within these organs.

Materials and Methods

Monte Carlo simulation proved to be an effective methodology for quantifying organ-specific dose deposition. To assess energy deposition within the brain tumor, the ORNL-MIRD phantom [30] was employed. Encompassing the entire tumor volume required extending the Bragg peak, resulting in the generation of multiple Bragg peaks at different energy levels. The study also analyzed and presented the flux and dose distribution of secondary particles. Furthermore, the total doses of secondary particles in both affected and unaffected organs were computed using GEANT4. These findings underscore the potential advantages of employing carbon ion therapy for brain tumor treatment.

The present study is divided into two main sections. The initial section introduces and simulates the ORNL-MIRD phantom using the GEANT4 framework. The subsequent section outlines the construction of the SOBP and computes the dose distribution necessary to cover the brain tumor. Additionally, this article investigates the secondary particles generated during carbon ion therapy.

Simulation methods

The GEANT4 toolkit serves as a versatile simulation tool for investigating particle-matter interactions. Its applications span a range of domains, including high-energy physics, nuclear physics, accelerator physics, and medical science, enabling the simulation of dose and flux pertaining to carbon ions. In this study, the GEANT4 toolkit release 4.11.0 was employed.

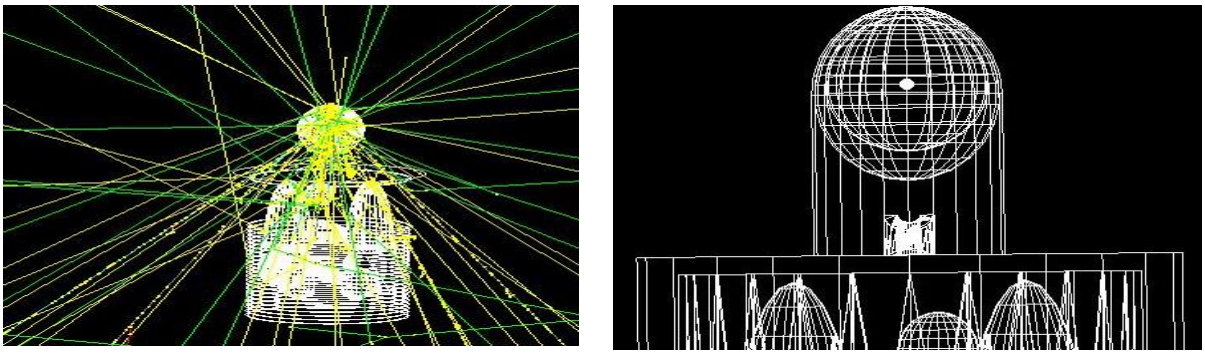

Figure1. Left) simulated human phantom and track of particles; Right) Head phantom with a centrally situated tumor phantom

Initially, a simulation of a 1 cm diameter spherical brain tumor within the ORNL-MIRD phantom computational model was conducted. Developed in the 1960s by researchers from the Oak Ridge National Laboratory (ORNL) and the Medical Internal Radiation Dose (MIRD) Committee, the ORNL-MIRD phantom is widely utilized in nuclear medicine and radiation dosimetry studies. It serves as a computational representation of the human body, incorporating mathematical models of organs, tissues, and skeletal structures. Constructed using anatomical and physiological data, these models realistically simulate radioactive substance distribution within the body, making the phantom essential in radiation dosimetry studies. This facilitates dose estimation for various organs and tissues during exposure to radioactive materials in medical imaging and cancer therapy. The tumor is located approximately 8-9 cm from the entrance surface. The material compositions of the head are detailed in the ICRU report [31]. Figure 1 depicts a simulated human phantom featuring a brain tumor. A circular disk with a 0.5 cm radius represents the carbon ion beam source for direct irradiation. Perpendicular to the phantom's head, the source is positioned 1 cm above the phantom, situated 95 cm from the world volume center along the z-axis. Employing the extensively validated QGSP_INCLXX reference physics list [32, 33], Bragg peaks were calculated at varying depths using mono-energetic carbon ion beams to cover the entire tumor. Subsequently, the SOBP was constructed, and the calculated energies and their probabilities were applied as the source beam to estimate dose distribution within different organs. Carbon energy deposition was computed, in 1 cm × 1 cm × 1 mm rectangular voxels, as a function of depth. The calculation relied on 10^7 primary carbon particles with an uncertainty of less than ~3 percent. A range cut-off value of 0.1 mm was set, defining secondary generation limits. Step max value for the calculation was 0.005 mm. Note that the smaller steps ensure higher precision but result in longer computation times. These Monte Carlo simulations were performed on an Intel Xeon computer featuring 48 processors at 3.6 GHz and 32 GB RAM memory, operating on a 64-bit system.

SOBP construction and calculation of dose distribution

In carbon therapy treatment planning, the Spread-Out Bragg Peak (SOBP) is utilized to administer a therapeutic radiation dose that comprehensively covers the entire tumor volume. This is pivotal, as relying solely on the Bragg peak may not adequately encompass the target region. For precise tumor targeting, the inclusion of multiple Bragg peaks at varying depths becomes imperative. Through the amalgamation of these peaks, the Spread-Out Bragg Peak (SOBP) is generated. This process involves superimposing the depth dose curves of carbon ions possessing differing energies. This strategic superposition yields a broader radiation distribution, effectively covering the complete tumor volume. Initially, the energy range requisite for precise tumor targeting is computed. Subsequently, a set of linear equations is employed to ascertain the weighting factors for each Bragg peak, which are crucial to achieve the desired radiation distribution within this energy spectrum. This meticulous determination of weights enables fine-tuned control over the SOBP's shape and intensity, ensuring that the tumor receives an efficacious dose while minimizing radiation exposure to adjacent healthy tissue. Following this, the creation of the SOBP within the brain tumor volume involves the summation of Bragg curves, utilizing calculated weighting factors according to Equation (1):

$$P_m=A_1P_1+A_2P_2+A_3P_3+\ldots+A_nP_n. \quad (1)$$

Here, P_1 to P_8 represent the curves, P_m signifies the SOBP curve, and A_1–A_8 denote the calculated weighting factors [29]. Within this paper, we computed proton, electron, neutron, and alpha depth dose and fluencies within both the tumor and the surrounding normal tissue. Finally, the cumulative deposited dose stemming from carbon ions and secondary particles was calculated within various body organs.

Results

Bragg Peaks and SOBP

To establish a Spread-Out Bragg Peak (SOBP), the initial phase involves identifying suitable carbon ion Bragg peaks within the treatment volume capable of generating an appropriate dose distribution in the tumor target. These Bragg peaks and their corresponding positions are

illustrated in Figure 2. Drawing insights from the data presented in Figure 2, the energy range for carbon ions falls within 2420 MeV to 2560 MeV. It's worth noting that carbon ions exhibit sharper and narrower Bragg peaks compared to protons. However, during their interactions with various tissues, carbon ions can undergo fragmentation into smaller secondary particles. These secondary fragments possess lower atomic numbers (Z) and longer ranges than primary carbon ions, leading to dose delivery beyond the Bragg peaks [34, 35]. The construction of the SOBP, using Equation (1) and incorporating weighting factors, is depicted in Figure 3 and Table 1.

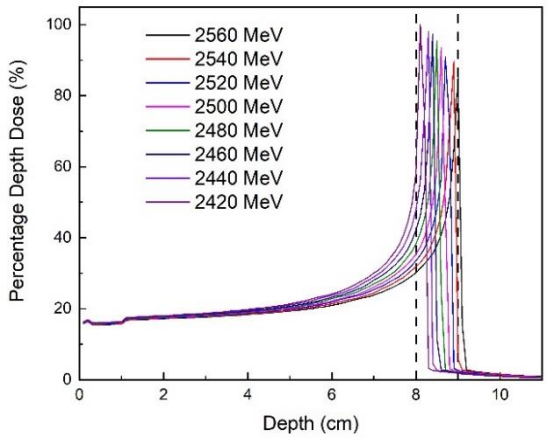

Figure 2. Bragg peaks to cover the brain tumor based on the depth.

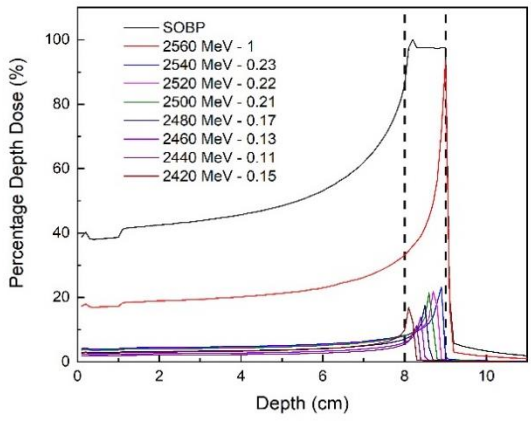

Figure 3. Constructed SOBP in the tumor target, the weighing factor presented in the legend.

The parameters of a formulated SOBP align with the beam specifications outlined by ICRU (2007). These SOBP parameters, encompassing penetration depth, distal dose fall-off, SOBP length, and target length, are discussed below [36].

In accordance with Table 2, the penetration depth (d'90) denotes the distance along the central beam axis to the distal 90% point of the maximum dose. The distal-dose fall-off (DDF) signifies the length interval where the dose, along the central beam axis, drops from 80% of the maximum dose to 20%. Additionally, m'90 represents the SOBP length, delineating the interval between the distal and proximal 90% points of the maximum dose. The target length is defined as the distance between a DDF length originating from the 90% proximal side of the maximum dose value and twice the DDF length from the distal 50% of the maximum dose value [29, 37]. For visualizing the dose distribution across the width, the dose profile of the SOBP is exhibited in Figure 4. Should the lateral dose manifest significantly, it can yield elevated doses in the healthy tissues adjacent to the target volume. The penumbra (80%–20%) and FWHM were computed as approximately 0.1 cm and 1 cm, respectively Table 2. The penumbra denotes the transverse width of the dose profile when the dose value descends from 80% to 20%. This parameter pertains to a collimated scattered carbon ion beam and hinges on the beam design and collimation systems [38].

Table 1. The optimized factors used to build SOBP.

Energy (MeV)	Weighting factor
2560	1.00
2540	0.23
2520	0.22
2500	0.21
2480	0.17
2460	0.13
2440	0.11
2420	0.15

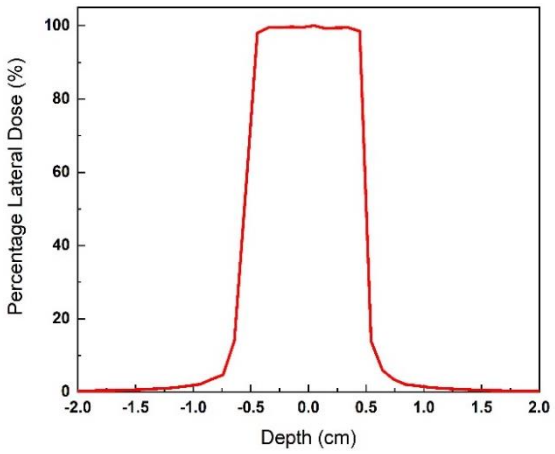

Figure 4. The lateral dose plot in the central depth of SOBP.

Secondary particles

The interactions between primary and secondary particles within body tissues yield a diverse array of particle formations. To comprehensively investigate the depth-dependent variations in dose deposition and flux, this study scrutinized the individual contribution of each secondary particle generated within each voxel. The considered secondary particles encompassed photons, neutrons, electrons, protons, and alphas. The reference framework adopted in this work was anchored to the head's entrance upper surface.

Table 2. Parameters used to characterize the carbon dose distribution for designed SOBP.

Parameters	d'90 (cm)	DDF (cm)	m'90 (cm)	Target length (cm)
Values	9	0.09	1.02	1.01

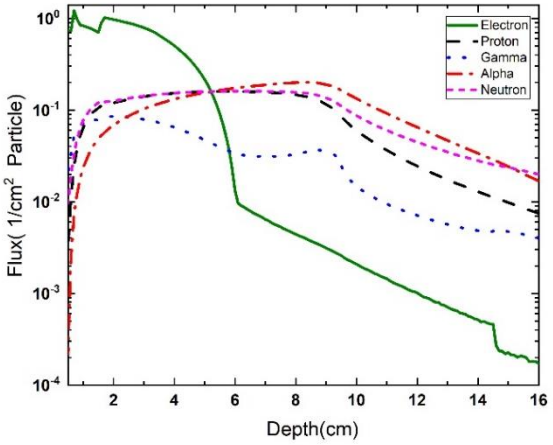

Figure 5. Secondary particles depth flux due to the Carbon ion interactions.

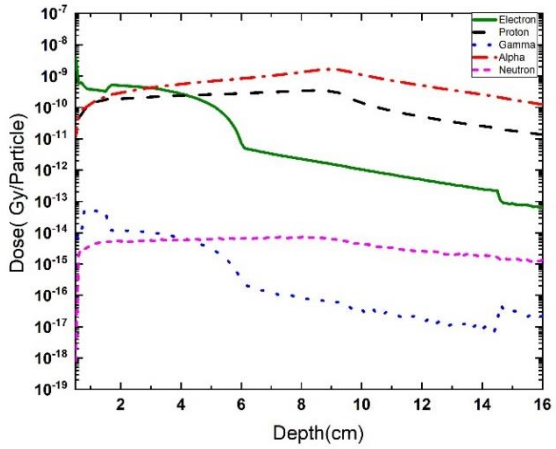

Figure 6. Secondary particles depth dose due to the Carbon ions interactions.

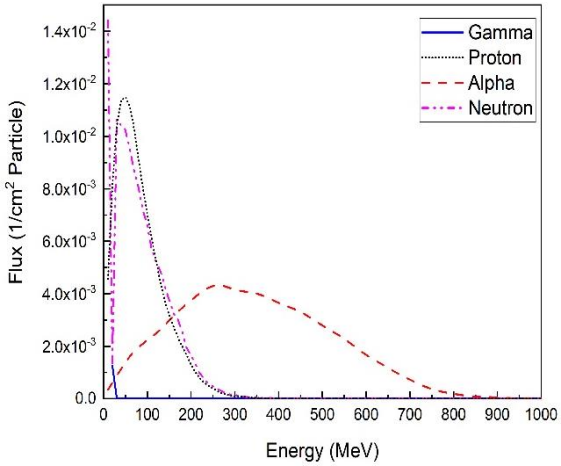

Figure 7. Secondary particles flux on the surface of the tumor.

The outcomes, manifesting as flux and dose curves of these secondary particles, are depicted in Figures 5 and 6, respectively. It's noteworthy that the entrance surface of the head could experience minor energy deposition from secondary particles, particularly those emerging from interactions with skull materials. Within this spectrum, alpha and proton particles exhibit more substantial contributions to deposited dose compared to others. Importantly, the dose attributed to gamma rays is approximately 10^7 times lower than that of protons. The flux curves on the tumor surface arising from secondary alpha particles, neutrons, protons, and photons are portrayed in Figure 7.

Discussion

Carbon therapy boasts the capacity to concentrate a substantial dose within the tumor region while mitigating harm to adjacent healthy tissue. Depth dose distributions were computed for diverse non-primary particles, including protons, neutrons, photons, and alphas, which exhibited a consistent pattern across these particles. Protons and alphas demonstrated higher deposited doses compared to other secondary particles. Simulations indicate that increased lateral doses could result in notable radiation exposure to the healthy tissues surrounding the targeted region. The influence of a high rate of secondary neutrons has been examined in carbon ion radiotherapy and proton therapy for liver cancer, prostate cancer, and pediatric brain tumors, involving both Monte Carlo simulation and experimental methods [29]. Figure 4 illustrates the dose profile of the SOBP, offering insight into dose distribution across its width. Two essential parameters, the penumbra and full-width at half-maximum (FWHM), serve to assess the precision and accuracy of radiation therapy treatments. The penumbra, crucial for collimated scattered carbon ion beams, signifies the transverse width of the dose profile where the dose value decreases from 80% to 20%. This metric hinges on the beam's design and collimation systems [36]. Importantly, increasing carbon beam energy leads to a shift of the alpha spectrum towards higher energies, with protons and neutrons displaying peaks at lower energies. The alpha spectrum peaks at an energy of approximately 250 MeV.

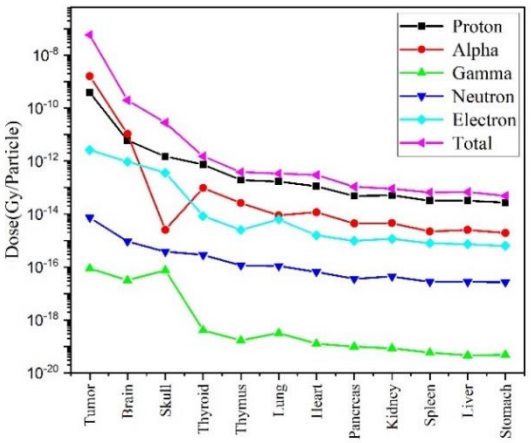

Figure8. Calculated total and secondary particles dose in different organs of the human phantom.

Table 3. Total dose in the organ name and RMS (%).

Organ name	Total dose(mGy)	RMS (%)
Brain	1.96131	0.005
Tumor	589.899	0.022
Heart	$3.03852*10^{-3}$	0.336
Thymus	$3.74856*10^{-3}$	0.812
Thyroid	$15.1549*10^{-3}$	0.545
Left lung	$1.67466*10^{-3}$	0.318
Right lung	$1.67878*10^{-3}$	0.318
Pancreas	$1.03508*10^{-3}$	1.041
Skull	$284.535*10^{-3}$	0.013
Spleen	$624.885*10^{-6}$	0.996
Stomach	$488.444*10^{-6}$	0.788
Liver	$666.282*10^{-6}$	0.361
Left kidney	$435.494*10^{-6}$	1.251
Right kidney	$443.449*10^{-6}$	1.250
Right adrenal	$673.656*10^{-6}$	3.175
Left adrenal	$650.145*10^{-6}$	3.273

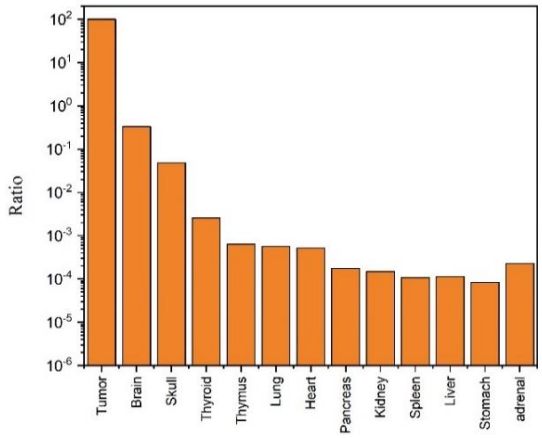

Figure 9. The ratio of the delivered dose in the body organs concerning the tumor dose.

Figure 8 visualizes the deposited dose in the tumor target and select non-involved organs within the human phantom. The specific organs featured in Figure 8 are listed in Table 3. Noteworthy is the minimal received dose in organs such as the liver, situated at a distance from the tumor region, as depicted. The study highlights that alpha particles yield higher doses in various organs relative to other particles, while gamma doses are comparably lower. The ratios of deposited dose across the 16 organs in relation to the tumor-delivered dose are presented in Figure 9. All body tissues experience radiation effects, with organs closer to the brain, like the brain and skull, receiving comparatively higher doses. Notably, ratios for organs such as the stomach, kidney, liver, and skull were approximately 8.36×10^{-7}, 1.55×10^{-6}, 1.16×10^{-6}, and 4.8×10^{-4}, respectively. Remarkably, the healthy brain's tissue area received a higher dose compared to other healthy organs, with a ratio of only 0.003 relative to the dose in the tumor region.

Conclusion

The primary goal of this study was to ascertain the optimal range of carbon ion energy for the effective treatment of brain tumors. Through meticulous calculations, it was determined that the energy interval most conducive to encompassing the brain tumor resided between 2420 and 2560 MeV. To ensure the precision of treatment administration, the SOBP technique was harnessed. This approach entailed harnessing diverse Bragg Peaks and skillfully optimizing weighting factors to attain comprehensive coverage of the brain tumor volume and attain the intended dose distribution within this region. Beyond the evaluation of the dose delivered to the tumor locale, the study undertook an estimation of the cumulative deposited dose in non-involved organs stemming from both carbon ions and secondary particles. Intriguingly, the ratios across various organs were notably diminutive, with the healthy brain tissue zone exhibiting a ratio approximately equal to 0.003. This observation suggests a slightly higher dose in this specific healthy brain tissue sector in comparison to other organs. Nevertheless, these ratios remained markedly low, underscoring that the delivered dose of carbon ions and associated non-primary particles within non-involved healthy tissues during brain carbon therapy is marginal and lacks significance. In sum, the outcomes strongly indicate that carbon ion therapy for brain applications stands as an efficacious treatment modality. It achieves precise dose delivery to the tumor while effectively minimizing radiation exposure to non-involved, healthy tissues. This insight underscores the potential of carbon ion therapy in the realm of brain tumor treatment, offering a promising equilibrium between targeted treatment efficacy and the safeguarding of vital healthy brain tissue.

References

1. Mitin T, Zietman AL. Promise and pitfalls of heavy-particle therapy. J Clin Oncol. 2014;32(26):2855.

2. Tommasino F, Scifoni E, Durante M. New ions for therapy. Int J Particle Ther. 2015;2(3):428-38.
3. Mihai M, Spunei M, Malaescu I. Comparison features for proton and heavy ion beams versus photon and electron beams. Rom Rep Phys. 2014;66(1):212-22.
4. Jiang F, Song YT, Zheng JX, Zeng XH, Wang PY, Zhang JS, Zhang WQ. Energy loss of degrader in SC200 proton therapy facility. Nucl Sci Tech. 2019;30(1):1-8.
5. Hong L, Goitein M, Bucciolini M, Comiskey R, Gottschalk B, Rosenthal S, et al. A pencil beam algorithm for proton dose calculations. Phys Med Biol. 1996;41(8):1305.
6. Jia Y, Beltran C, Indelicato DJ, Flampouri S, Li Z, Merchant TE. Proton therapy dose distribution comparison between Monte Carlo and a treatment planning system for pediatric patients with ependymoma. Med Phys. 2012;39(8):4742-7.
7. Larsson B. Proton and heavy ion therapy. In: Seventh International Conference on Cyclotrons and their Applications; 1975; Basel, Switzerland. Birkhäuser; 1975. p. 414-8.
8. Enferadi M, Sarbazvatan S, Sadeghi M, Hong JH, Tung CJ, Chao TC, Wey SP. Nuclear reaction cross sections for proton therapy applications. J Radioanal Nucl Chem. 2017;314(2):1207-35.
9. Mahdipour SA, Mowlavi AA. Ion therapy for uveal melanoma in new human eye phantom based on GEANT4 toolkit. Med Dosim. 2016;41(2):118-25.
10. Bagheri R, Moghaddam AK, Azadbakht B, Akbari MR, Shirmardi SP. Determination of water equivalent ratio for some dosimetric materials in proton therapy using MNCPX simulation tool. Nucl Sci Tech. 2019;30(2):31.
11. Koto M, Demizu Y, Saitoh JI, Suefuji H, Tsuji H, Okimoto T, et al. Multicenter study of carbon-ion radiation therapy for mucosal melanoma of the head and neck: subanalysis of the Japan Carbon-Ion Radiation Oncology Study Group (J-CROS) study (1402 HN). Int J Radiat Oncol Biol Phys. 2017;97(5):1054-60.
12. Schulz-Ertner D, Jäkel O, Schlegel W. Radiation therapy with charged particles. Semin Radiat Oncol. 2006;16(4):249-59.
13. Amaldi U, Kraft G. Radiotherapy with beams of carbon ions. Rep Prog Phys. 2005;68(8):1861.
14. Soltani-Nabipour J, Popovici MA, Strasser L, Cata-Danil GH. Bragg peak shape parameters as a tool for improving the I-value estimation. Rom Rep Phys. 2011;63(3):651-75.
15. Mohamad O, Sishc BJ, Saha J, Pompos A, Rahimi A, Story MD, et al. Carbon ion radiotherapy: a review of clinical experiences and preclinical research, with an emphasis on DNA damage/repair. Cancers. 2017;9(6):66.
16. Allen C, Borak TB, Tsujii H, Nickoloff JA. Heavy charged particle radiobiology: using enhanced biological effectiveness and improved beam focusing to advance cancer therapy. Mutat Res Fundam Mol Mech Mutagen. 2011;711(1-2):150-7.
17. Paganetti H, editor. Proton therapy physics. CRC Press; 2018.
18. Verburg JM, Grassberger C, Dowdell S, Schuemann J, Seco J, Paganetti H. Automated Monte Carlo simulation of proton therapy treatment plans. Technol Cancer Res Treat. 2016;15(6):NP35-46.
19. Allison J, Amako K, Apostolakis JE, Araujo HAAH, Dubois PA, Asai MAA, et al. Geant4 developments and applications. IEEE Trans Nucl Sci. 2006;53(1):270-8.
20. Kawrakow I. Accurate condensed history Monte Carlo simulation of electron transport. I. EGSnrc, the new EGS4 version. Med Phys. 2000;27(3):485-98.
21. Hendricks JS, McKinney GW, Fensin ML, James MR, Johns RC, Durkee JW, et al. MCNPX 2.6.0 extensions. Los Alamos National Laboratory; 2008. Report No.: 73.
22. Agostinelli S, Allison J, Amako KA, Apostolakis J, Araujo H, Arce P, et al. GEANT4—a simulation toolkit. Nucl Instrum Methods Phys Res A. 2003;506(3):250-303.
23. Ying CK, Kamil WA, Shuaib IL, Matsufuji N. An improved Monte Carlo (MC) dose simulation for charged particle cancer therapy. In: AIP Conference Proceedings; 2014 Feb; 1584(1):97-100. American Institute of Physics.
24. Cirrone GAP, Cuttone G, Mazzaglia ES, Romano F, Sardina D, Agodi C, et al. Hadrontherapy: a Geant4-based tool for proton/ion-therapy studies. Prog Nucl Sci Technol. 2011;2:207-12.
25. Kraft G. Tumor therapy with ion beams. Nucl Instrum Methods Phys Res A. 2000;454(1):1-10.
26. Matsumoto S, Yonai S, Bolch WE. Monte Carlo study of out-of-field exposure in carbon-ion radiotherapy: organ doses in pediatric brain tumor treatment. Med Phys. 2019;46(12):5824-32.
27. Demizu Y, Jin D, Sulaiman NS, Nagano F, Terashima K, Tokumaru S, et al. Particle therapy using protons or carbon ions for unresectable or incompletely resected bone and soft tissue sarcomas of the pelvis. Int J Radiat Oncol Biol Phys. 2017;98(2):367-74.
28. Makishima H, Yasuda S, Isozaki Y, Kasuya G, Okada N, Miyazaki M, et al. Single fraction carbon ion radiotherapy for colorectal cancer liver metastasis: a dose escalation study. Cancer Sci. 2019;110(1):303-9.
29. Ganjeh ZA, Eslami-Kalantari M, Mowlavi AA. Dosimetry calculations of involved and noninvolved organs in proton therapy of liver cancer: a simulation study. Nucl Sci Tech. 2019;30(12):1-7.
30. Han EY, Bolch WE, Eckerman KF. Revisions to the ORNL series of adult and pediatric computational phantoms for use with the MIRD schema. Health Phys. 2006;90(4):337-56.
31. White DR, Booz J, Griffith RV, et al. Report 44. J Int Comm Radiat Units Meas. 2016;OS23:NP-NP.
32. Amako K, et al. Comparison of Geant4 hadronic models with experimental data in the energy range 0.1-12 GeV. Nucl Instrum Methods Phys Res B. 2008;266(3):408-21.
33. Garcon MV, Watson JW. The Intranuclear Cascade Model for High-Energy Nuclear Collisions. Prog Part Nucl Phys. 1993;30(1):49-91.
34. Sangwan N, Kumar A. An extensive study of depth dose distribution and projectile fragmentation cross-section for shielding materials using Geant4. Appl Radiat Isot. 2021;110068.
35. Ahmadi Ganjeh Z, Eslami-Kalantari M, Mowlavi AA. The effect of phantom compositions on dose calculations in proton therapy of liver cancer. J Arak Univ Med Sci. 2020;22(6):274-87.

36. International Commission on Radiation Units and Measurements (ICRU). Prescribing, Recording, and Reporting Proton-Beam Therapy. ICRU Report 78. 2007.
37. Rasouli FS, Masoudi SF, Keshazare S, Jette D. Effect of elemental compositions on Monte Carlo dose calculations in proton therapy of eye tumors. Radiat Phys Chem. 2015;117:112-9.
38. Suit H, DeLaney T, Goldberg S, Paganetti H, Clasie B, Gerweck L, et al. Proton vs carbon ion beams in the definitive radiation treatment of cancer patients. Radiother Oncol. 2010;95(1):3-22.